UNIVERSITY OF BIRMINGHAM

Research at Birmingham

Performance assessment of a nuclear waste repository: Upscaling coupled hydro-mechanical properties for far-field transport analysis

Blum, Philipp; Mackay, Rae; Riley, Michael; Knight, JL

Document Version
Publisher's PDF, also known as Version of record

Link to publication on Research at Birmingham portal

Performance assessment of a nuclear waste repository: Upscaling coupled hydro-mechanical properties for far-field transport analysis

P. Blum[a,1], R. Mackay[a,*], M.S. Riley[a], J.L. Knight[b]

[a]*Hydrogeology Research Group, Earth Sciences, School of Geography, Earth and Environmental Sciences, University of Birmingham, Edgbaston, Birmingham B15 2TT, UK*
[b]*United Kingdom Nirex Ltd., Curie Avenue, Harwell, Didcot, Oxon OX11 0RH, UK*

Abstract

A methodology for addressing the DECOVALEX III Bench Mark Test 2 is presented. Hydro-mechanical (HM) modelling has been conducted on fracture networks generated from fracture length and density statistics, which have been described by a power law. For each rock formation in the test, effective hydraulic conductivity tensors have been derived for a range of mechanical parameters and depths below ground level. The upscaled hydraulic conductivities have been used in a site scale continuum model of groundwater flow and transport to assess performance indicators, including time of travel from repository to ground surface. Preliminary results indicate that interpretation of the fracture length and density data can have a significant effect on upscaling calculations, including the determination of a suitable hydraulic representative elementary volume. HM modelling shows that there is a non-linear decrease in the change of fracture aperture with depth, and that although large aperture fractures remain at depth, the majority of fractures tighten to almost the residual aperture at about 750 m below ground level. Consequently, anisotropy of the effective hydraulic conductivity also changes with depth. Flow and transport modelling at the field scale indicates that, of the controls investigated, mechanical properties of the rock have the greatest influence on solute travel times.
© 2005 Elsevier Ltd. All rights reserved.

1. Introduction

Continuum models of sub-surface flow and transport have been used to provide predictions for the performance assessment of underground radioactive waste disposal for many years. As awareness of relevant host rock processes has increased, these models have become increasingly sophisticated. Their structure and parameterisation typically reflects data collected at spatial scales that are usually orders of magnitude smaller in volume than those over which the prediction of radionuclide migration is required. Upscaling is, therefore, required

by default for the successful application of the models. Formal upscaling methods are increasingly used to transform the small-scale data into large-scale values required as input to numerical models [1]. Although many upscaling strategies have been proposed (including that of Jackson et al. [2]), the problem of translating the information contained in field data into meaningful continuum model parameters remains contentious. The problem not only involves transformation of scale, but also includes the interpolation/extrapolation of parameter values determined at specific locations in the rock, for example near a borehole or at outcrop, to locations throughout the rock including areas where ambient conditions may be significantly different. One particular issue of concern is the effect of the variation with depth of the mechanical stress field on the hydraulic properties of a formation and the consequent effect on the groundwater flow-mediated time of travel from a waste

*Corresponding author. Tel.: +44 121 414 6142;
fax: +44 121 414 4942.

E-mail address: r.mackay@bham.ac.uk (R. Mackay).
[1]Present address: URS Deutschland GmbH, Hauptstrasse 45a, D-30974 Wennigsen, Germany.

repository at depth to the surface. The international collaborative programme, DECOVALEX III, was set up in part to address this and related issues, with particular emphasis on an evaluation of coupled thermo-hydro-mechanical processes for performance assessment of potential buried radioactive waste disposal sites.

As part of the DECOVALEX III programme, several research teams have independently tackled a two-dimensional (2D) upscaling problem based upon a hypothetical deep waste disposal scenario (Bench Mark Test 2). In this paper, the approach taken by the authors to solve this problem is described and the preliminary results presented.

Fig. 1 shows the hypothetical repository situated within a low permeability fractured rock mass (Formation 1), which is overlain by an upper fractured formation (Formation 2) that extends to ground surface. A vertical fractured/faulted zone cuts both rock units (The Fault Zone). This zone lies just beyond the end of the repository tunnel. The repository is backfilled with a low permeability bentonite seal. The rock property data for each formation and the fault zone are based on the Sellafield (Cumbria, UK) site investigation programme performed by United Kingdom Nirex Limited, but the spatial distribution of the formations has been substantially modified from that found at Sellafield. Thus, the results presented in this paper, and under DECOVALEX III Bench Mark test 2 as a whole, cannot be used to infer any knowledge of the real conditions at Sellafield. The 2D model domain corresponds to a vertical section, 5 km long and 1 km deep, that intersects the coastline. The land surface onshore is low-lying and offshore the seabed is shallow. The orientation of the 2D cross-section through the host rock is NNW/SSE (159/339°). The repository is located at a depth of 520 and 10 m NNW from the fault zone, which penetrates from ground surface to the base of the section. Hydraulically, the base and sides of the model domain are represented as no flow boundaries, and the top boundary is prescribed by a constant pressure set equal to atmospheric pressure, fixing the water table at the ground surface everywhere. Density variations in the groundwater salinity composition are not considered in the hypothetical scenario.

The methodology described in this paper (Fig. 2) has been implemented to quantify the background variations of the host rock hydraulic properties as a function of the in situ stresses and mechanical properties. A similar methodology has been used by Martin et al. [3], who applied it to assess a major shear zone in granite, and Eidsvig [4] who used it to describe the stress-dependent permeability in fractured chalk. An incentive for the development of the methodology is that, potentially, it makes it possible to examine fault zones and to explain the depth distributions of flowing features observed during the Sellafield site investigation programme [5]. The methodology comprises four main stages.

Stage 1 concerns the statistical analysis of the given fracture distribution data and the generation of synthetic discrete fracture networks (DFNs). The uncertainties in the parameterisation of the fracture length and density data are examined and their effect on the simulated networks is highlighted.

Stage 2 comprises hydraulic and mechanical analysis of permeability. The purpose of stage 2 is to establish the minimum size of averaging volume (denoted here as the approximate REV) required to model large-scale
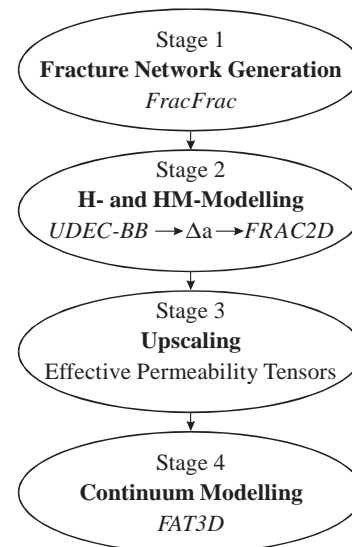

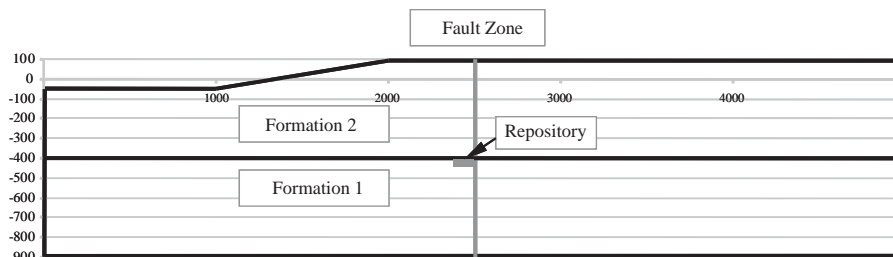Fig. 2. Overall modelling strategy (Δa = hydraulic aperture change).

Fig. 1. Modelling domain defined by the DECOVALEX III reference problem.

flow, the hydro-mechanical (HM) contributions to the equivalent continuum permeability tensor at the approximate REV scale, and the statistical variability in the upscaled parameter values. Several methods exist to evaluate the 2D permeability tensor for fractured rock e.g. [6,7]. In this paper the evaluation is based on the work of Jackson et al. [2], which models flow through a block of fractured rock in several directions using boundary conditions that impose a uniform head gradient on the block, and which are set beyond the limits of the REV. The impact of HM interactions on the permeability tensor is explored by numerically modelling the changes in hydraulic aperture distribution, given data on the fluid and rock stress distributions, and establishing a modified permeability tensor. Sensitivity studies using the distinct element code, UDEC, incorporating the Barton Bandis model for mechanical fracture closure (UDEC–BB) are used to examine the impact of mechanical properties, stress changes with depth, mechanical boundary conditions, and fracture geometries, and to determine a suitable REV for HM modelling.

Stage 3 uses the results of the calculations carried out during Stage 2 to constrain upscaling calculations of effective flow and advective transport parameters for cells of a finite difference continuum model of the hypothetical site.

Stage 4 involves the full continuum modelling of the regional groundwater flow patterns within a Monte-Carlo simulation framework. The distributions of effective parameters derived in Stage 3 are sampled to construct alternative realisations of the permeability and porosity fields in the 2D domain. The finite difference model is then used to simulate flow through the host formations and to estimate performance measures such as the advective travel time from the repository to the surface for each realisation. This allows the effect of fracture geometry, and mechanical properties on performance assessment measures to be investigated quantitatively.

2. Methodology and preliminary calculations

2.1. Fracture data and fracture generation

The most abundant data for DFN generation (Stage 1) are fracture density and length [7]. A power law fracture length distribution has been fitted to the available data as shown in Fig. 3. The number of fractures per km^2 (N_F) longer than the length (L) measured in metres is given by

$$N_F = CL^{-D}, \qquad (1)$$

where C is a density constant and D is the fractal dimension. The data include only fractures with a length
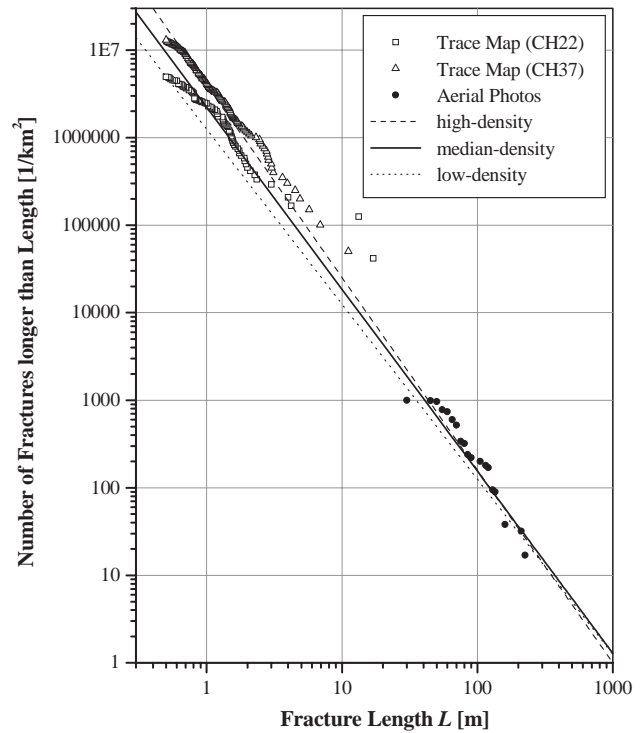

Fig. 3. Power law distribution of fracture length (based on Nirex [7]).

greater than a lower cut-off length of 0.5 m. The magnitude of the lower cut-off length governs the fracture density for a given C and D. The data set in Fig. 3 can be modelled plausibly using a range of values of C and D, resulting in a range of possible fracture network densities. Three density cases, which sensibly fit the data, were chosen for comparison (low density: $C = 1.25$, $D = 2.0$; medium density: $C = 3.23$, $D = 2.08$; high density: $C = 4.0$, $D = 2.2$). The mean fracture densities (P_{21}) of 5.0, 13.2 and 16.9 m/m^2 for the low, medium and high-density cases, respectively, are illustrated in Fig. 4. They show the sensitivity of the simulated network to the choice of power law length distribution. Realisations of fracture length were constructed by sampling the power law cumulative distribution function

$$F(L) = 1 - \left(\frac{L}{L_{\min}}\right)^{-D}, \qquad (2)$$

where L is the fracture length and $L_{\min}$ is the lower cut-off length. The locations of the fracture centres were modelled using a simple Poisson distribution model. Although fracture separations are probably related to fracture length, this attribute of the real fracture networks has not been captured in the alternative realisations. Additionally, the dispersion of fracture orientations observed in the available data has not been included in the model. Calculated values of the Fisher
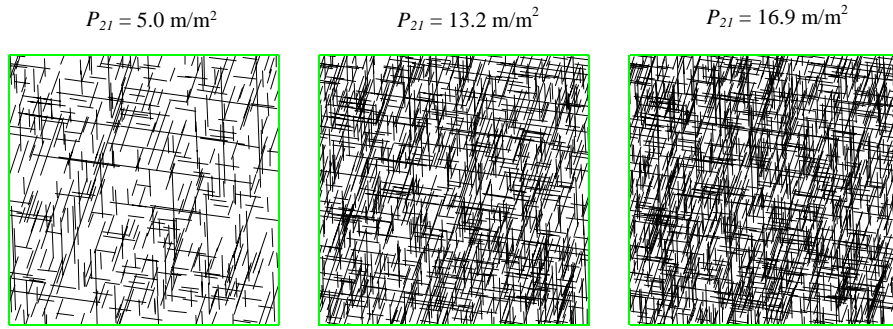
$P_{21} = 5.0 \, \text{m/m}^2$　　　　　$P_{21} = 13.2 \, \text{m/m}^2$　　　　　$P_{21} = 16.9 \, \text{m/m}^2$

Fig. 4. $10 \, \text{m} \times 10 \, \text{m}$ fracture networks with different fracture densities and a power law length distribution.

distribution coefficient obtained from analysis of the data lead to unrealistic images of the fracture networks. This appears to be related to a correlation between orientation and fracture length, whereby small fractures show greater dispersion about their mean orientation compared with the longer fractures. For each formation, one horizontal fracture set and two sub-vertical sets have been modelled. Data on the densities and fracture length distributions were not available to characterise each data set independently, and so data from all fracture sets in a formation were pooled and the derived parameter values used for the DFN generation.

2.2. Determination of effective flow and advective transport parameters

The initial hydraulic analysis incorporating a baseline REV determination was performed with the fracture flow code FRAC2D using DFNs with constant hydraulic aperture ($a_h = 130.7 \, \mu\text{m}$). To evaluate the equivalent 2D permeability tensor for square domains the boundary conditions were adjusted to give unit head gradients with directions ranging between $0°$ and $150°$ in $30°$ steps. The specific discharges (q_x and q_y) across the domain boundaries were calculated for each gradient direction assuming Darcian flow. The three hydraulic conductivity tensor components, K_{xx}, K_{yy} and K_{xy}, were estimated by minimising the expression:

$$\sum_{i=1}^{6} [(q_x)_i + (K_{xx} \cos \varphi_i + K_{xy} \sin \varphi_i)]^2 \\ + [(q_y)_i + (K_{xy} \cos \varphi_i + K_{yy} \sin \varphi_i)]^2, \qquad (3)$$

where φ_i is the direction of the hydraulic gradient. Fracture network generation regions of $100 \, \text{m} \times 100 \, \text{m}$ were adopted from which DFNs of 5–$100 \, \text{m}$ square were sampled. Numerous simulations were performed for each domain size and the principal hydraulic conductivity components, $K_{\max}$ and $K_{\min}$, and major principal direction, $\theta_{\max}$, were calculated. Fig. 5 illustrates graphically the results for one domain size. For the low-density case, 100 simulations were required to achieve acceptable convergence of the sample mean
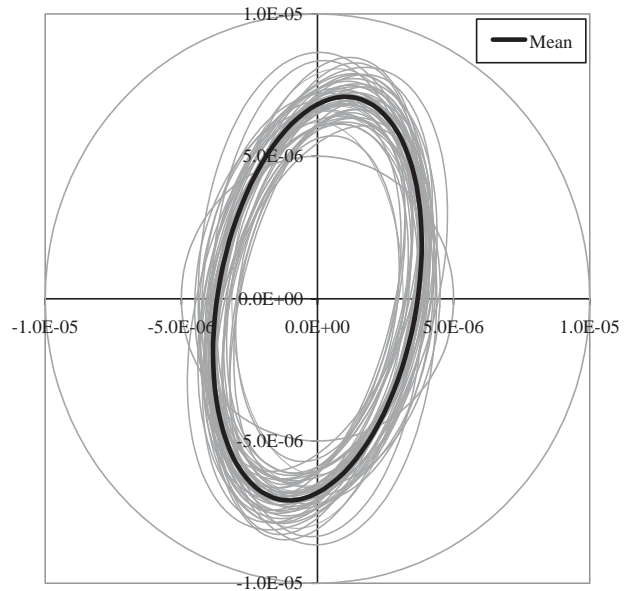

Fig. 5. Hydraulic conductivity ellipses from 50 simulations for the median fracture density case with a domain size of $10 \, \text{m} \times 10 \, \text{m}$ (scale represents hydraulic conductivity in m/s).

and standard deviation of the permeability components and orientation, while only 50 simulations were necessary for the medium and high-density cases. Fig. 5 illustrates the permeability anisotropy, which is caused by the two sub-vertical fracture sets having the highest fracture density.

The REV for the study is defined as the equivalent block scale at which it may be assumed that continuum approximations are applicable. This definition is imprecise and therefore the criteria used to define the REV scale for each formation are subjective and are based upon minimisation of the variance of the upscaled property values. For this study, the sample standard deviation of the principal permeability components and the principal directions must be less than 5% of their sample averages, before the domain size used for their calculation can be defined as above or at the size of the REV. The smallest domain size complying with these criteria is the minimum REV size. The application of

these criteria showed that for the medium and high-density cases all domain sizes greater than $10\,\mathrm{m} \times 10\,\mathrm{m}$ were above the minimum REV size. However, for the low-density case no REV was achieved up to a domain size of $100\,\mathrm{m} \times 100\,\mathrm{m}$ (the largest size that could be accurately modelled with FRAC2D). This is a consequence of the decreased connectivity in the minor flow direction for this case. The change of connectivity with fracture density also causes a rotation of the principal directions of conductivity with increasing domain size.

The effective porosity in fractured media has been calculated using the following equation:

$$n_{\mathrm{e}} = \frac{\hat{t}}{s}\,q, \tag{4}$$

where q is specific discharge, s is travel distance and $\hat{t}$ is mean travel time. For this study, the effective porosity has been assumed to be independent of the flow direction [8], although anisotropy has been observed during the calculations. The mean travel time is calculated across the DFN considering all pathways through the fracture network. The number of pathways for sizeable networks is prohibitively large. Particle tracking approaches are commonly used but these tend to consider only the most likely paths since the number of particles is usually orders of magnitude smaller than the number of alternative pathways. To avoid the approximation required by particle tracking, an algorithm has been developed that minimises the size of the travel time calculation whilst sampling all pathways, by integrating travel times calculated over connected sub-domains. This algorithm is able to return the mean travel time accurately and is sufficient for the calculation of an effective porosity, but does not provide data on dispersion through the fracture network.

2.3. HM modelling

HM analysis has been considered only for the medium fracture density case. The HM modelling was performed with the empirical UDEC–BB (Barton-Bandis) model [9,10]. The in situ stress field (MPa) is described by:

$$\sigma_{\mathrm{V}} = 0.0294\,d + 0.26622,$$
$$\sigma_{\mathrm{H}} = 0.03113\,d + 1.88747, \tag{5}$$

where σ_{V} is vertical stress, σ_{H} is horizontal stress and d is depth in metres below ground level [11].

For HM modelling, data sets are required that describe the rock block material and the joint material. Isotropic elastic behaviour is assumed for the rock blocks. The data set of joint roughness coefficient (JRC) and joint compressive strength (JCS) [12] shows major variations in measured values (Fig. 6) with no obvious relationships observable between JRC, JCS and depth. Four JRC/JCS parameter sets have been identified (denoted by open symbols in Fig. 7) and have been used to assess the sensitivity of the BB model to mechanical properties. For Formation 1, these represent a mean pair of values (set 1) and three cases including extreme values. For Formation 2, only four points are available and so all four have been used. A mean pair of values has been used to represent the fault zone. Data describing the uniaxial compressive strength of the rock block (UCS) are available in summary form only [11]. For the majority of simulations, the mean value for each formation was used. However, for the high JCS case in Formation 1 the maximum UCS value was used to fulfil the condition that the UCS must be greater than the JCS. The parameter values used in the BB model are summarised in Table 1. The shear data are not presented
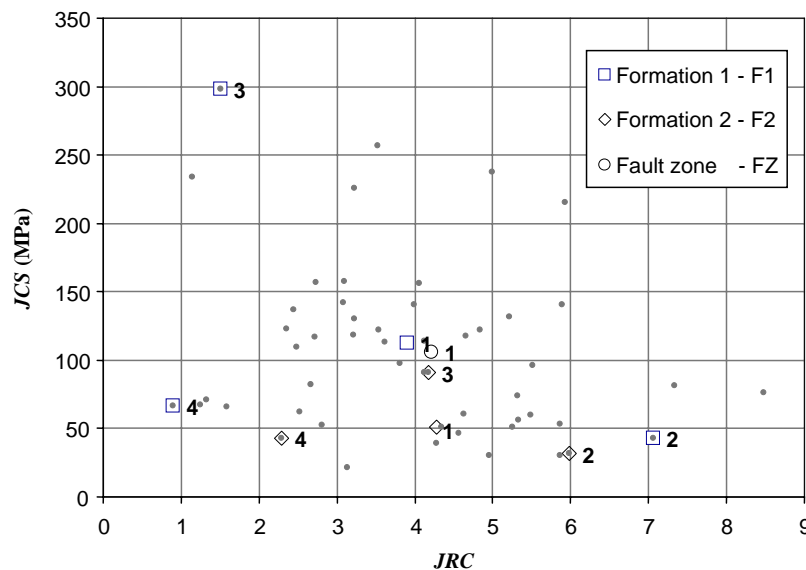

Fig. 6. Mechanical boundary conditions for the HM analysis with the block-in-block method.
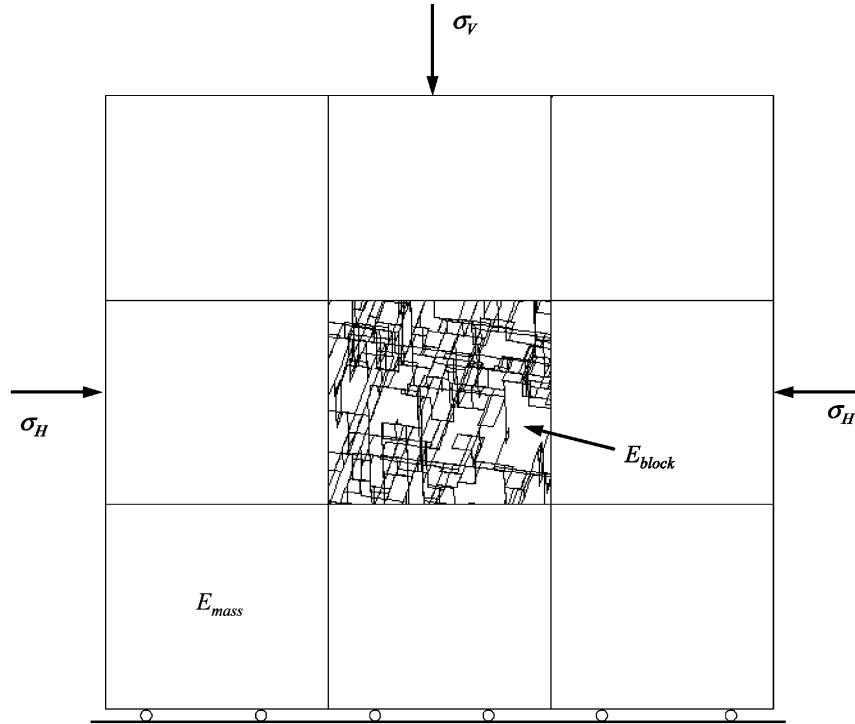
Fig. 7. *JRC* versus *JCS* (data from NGI [12]).

Table 1
UDEC–BB mechanical model parameters

Formation	Parameter set	JRC (−)	JCS (MPa)	UCS (MPa)	E_{block} (GPa)	Density (kgm^{-3})	Poisson ratio
F1	1	3.85	112.2	157.0	84.0	2750	0.24
	2	7.10	43.1	157.0			
	3	1.51	298.4	308.8			
	4	0.90	66.4	157.0			
F2	1	4.18	51.3	39.6	72.0	2650	0.24
	2	5.98	31.9				
	3	4.18	90.9				
	4	2.29	43.1				
FZ	1	4.22	105.9	128.4	60.0	2730	0.23

here as these were observed to be unimportant for the stress conditions applied for the simulations presented in this paper. The model requires an initial mechanical aperture, representing the fracture aperture under conditions of zero normal stress. This value, in microns, is calculated with the following empirical expression:

$$a_{ini} = 200JRC_0 \left(0.2 \frac{UCS}{JCS_0} - 0.1 \right), \tag{6}$$

where JRC_0 is the joint roughness coefficient at zero normal stress and JCS_0 is the joint compressive strength at zero normal stress [9].

Fig. 7 illustrates the applied mechanical stress field for the HM modelling. Fluid pressure is assumed to be hydrostatic. The bottom boundary is fixed in the y-direction, but all other mechanical boundaries are free to move. Primarily to reduce the impact of the bottom boundary constraint on the test block, the fracture network was located in the centre of eight blocks with uniform material properties characteristic of a jointed rock mass. Hence, the surrounding blocks were assigned a Young's modulus, E_{mass}, representative of the behaviour of the bulk rock, whereas the value for the intact rock, E_{block}, was used in the BB calculations for the central block. The name 'block-in-block' method has been coined for this approach. The results of the block-in-block configuration were tested against the case in which the boundary conditions are applied directly to the test block. The resulting median hydraulic apertures are modified slightly by this approach: for a 5 m × 5 m

block, the single block method yielded a median aperture of 22.4 μm, while the block-in-block method produced a value of 24.3 μm. Since it employs boundary conditions more representative of the in situ state of the rock, the block-in-block method has been used for all subsequent calculations.

Fracture aperture is significantly controlled by fracture orientation, Fig. 8, and leads to enhanced anisotropy of the upscaled hydraulic conductivity. As anticipated, the high *JRC* case produces the largest hydraulic apertures while the smallest hydraulic apertures are observed for a low *JCS* value and low *JRC* value combination.

Initial simulations of Formation 1 with mechanical parameter set 1, conducted to assess the effect on hydraulic aperture of increasing stress with depth below ground surface, indicate that changes to the distribution of the hydraulic apertures progressively decrease with depth (Fig. 9). There is almost no difference between the calculated aperture distributions at 750 m and at 1000 m depth: a residual hydraulic aperture distribution is achieved at around 750 m below ground level. The anisotropy in the aperture distribution, apparent near

the surface, is removed between depths of 250 and 500 m. At depths less than 250 m, the anisotropy can have a substantial impact on the magnitude of the permeability and the principal direction.

Finally, the sensitivity of fracture aperture to block size and fracture length was analysed. Fracture networks with domain sizes of 5 m × 5 m and 10 m × 10 m revealed differences in median hydraulic apertures of less than 0.5 μm. Even with a block size of 15 m × 15 m and effectively infinitely long fractures, the change in median hydraulic aperture remained less than 1 μm. It can be concluded that the size of the REV determined for flow only is also suitable for mechanical calculations, and that, for the assumed spatial distribution and orientation of fracturing, fracture length has only a minor impact on the hydraulic aperture distribution.

3. Block scale results of HM modelling

In the work presented here, only one DFN has been used for each formation. More wide-ranging Monte Carlo simulations are currently underway, but it appears, from preliminary simulations, that the overall sensitivity of the medium fracture density case results to network geometry are not strong in comparison to their sensitivity to mechanical parameters and to depth.

For HM modelling, alternative stress conditions corresponding to five depths were applied to the DFN. Table 2 summarises the HM modelling results in terms of the median hydraulic apertures. Values range between 0.05 and 180.7 μm. Considerable variability in fracture aperture is apparent and large apertures are simulated even at depths of 500–1000 m as observed in actual fractured rock at depth [13,14].

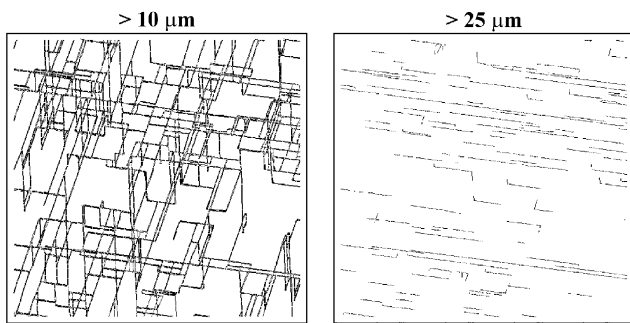The permeability tensors resulting from the HM modelled aperture distributions, using parameter set 1

Fig. 8. Aperture anisotropy for a fracture network at 50 m depth. Left: backbone fractures with $a_h > 10$ μm, right: backbone fractures with $a_h > 25$ μm.
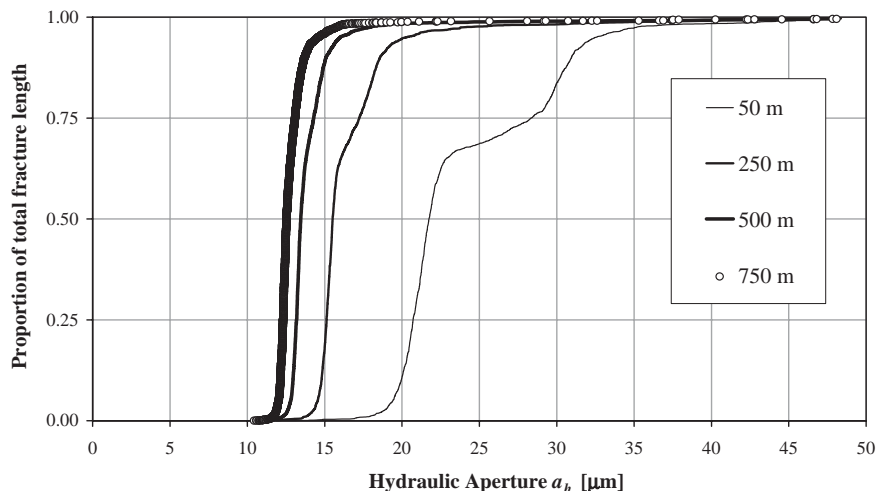

Fig. 9. Cumulative distributions of hydraulic aperture for a single fracture network as a function of depth below ground level.

for each formation, are presented in Table 3 in terms of the maximum hydraulic conductivity, anisotropy ratio and major principal direction. The results are illustrated for the fault Zone in Fig. 10. For comparison, Fig. 11 shows the effective hydraulic conductivity ellipses for the three rock formations for the purely hydraulic case with constant, arbitrary, fracture apertures of 50 μm. At depths less than 100 m, the major principal direction is aligned with the sub-horizontal fractures. With increasing depth, the major principal direction and the anisotropy gradually approach the values of the constant hydraulic case (Fig. 11) due to the convergence of the aperture distributions of all fractures towards a uniform value approximately equal to the residual aperture. The principal directions and anisotropy ratios for the other two formations display similar trends (Table 3).

Table 4 summarises the calculated mean effective porosities for the mean mechanical property case.

4. Site scale transport modelling

4.1. Hydraulic base case

All upscaled continuum modelling was performed with the flow and transport code FAT3D. For the

hydraulic case (H), three particle trajectories are used to illustrate the flow system. Two starting points are located at the ground surface at the right-hand side of the model domain to present the general flow regime in the system. The third trajectory is initiated at the NNW corner of the repository. All particle trajectories are calculated assuming advection only.

For the hydraulic base case, various constant hydraulic apertures and fracture densities were considered. Homogeneous hydraulic conductivity tensors and porosities were applied to each formation. The case with a constant hydraulic aperture of 10 μm and medium fracture density for all formations is illustrated in Fig. 12, where the streamlines and the particle travel times are shown. The time of travel between each marker is 1000 days. The streamline direction in the
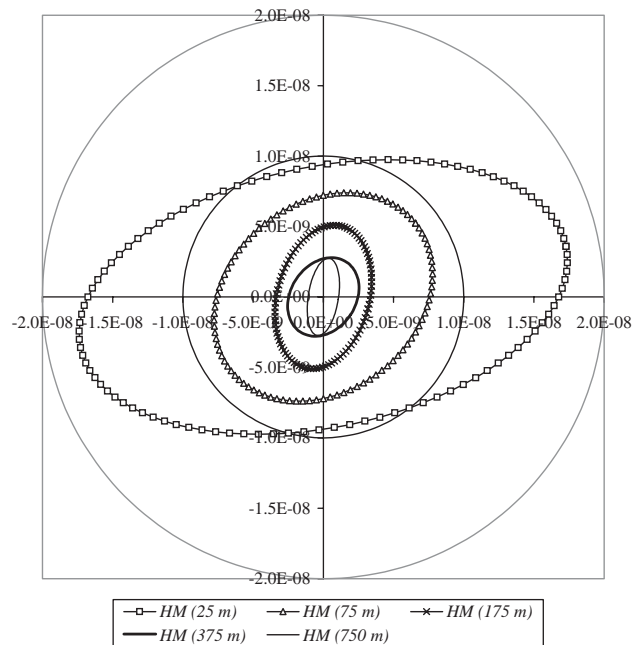

Fig. 10. HM-modified hydraulic conductivity ellipses for the fault zone.

Table 2
HM modelling results (median hydraulic apertures in μm)

	Depth:	25 m	75 m	175 m	375 m	750 m
Formation	Parameter set					
F1	1	27.3	22.1	18.0	15.0	13.2
	2	—	—	—	—	180.7
	3	—	—	—	—	1.7
	4	—	—	—	—	18.2
F2	1	0.56	0.27	0.12	0.05	—
FZ	1	18.2	14.9	12.6	10.9	9.8

Table 3
HM-modified hydraulic conductivity tensors for mechanical parameter set 1

	Depth:	25 m	75 m	175 m	375 m	750 m
Formation						
F1	K_{max} (ms^{-1})	—	—	—	—	5.9×10^{-9}
	K_{max}/K_{min}	—	—	—	—	2.1
	θ_{max} (°)	—	—	—	—	65.7
F2	K_{max} (ms^{-1})	1.4×10^{-12}	1.8×10^{-12}	2.6×10^{-14}	1.6×10^{-14}	—
	K_{max}/K_{min}	1.7	9.4	3.0	9.7	—
	θ_{max} (°)	38.2	87.1	53.7	39.5	—
FZ	K_{max} (ms^{-1})	1.8×10^{-8}	8.4×10^{-9}	5.2×10^{-9}	3.0×10^{-9}	2.8×10^{-9}
	K_{max}/K_{min}	1.9	1.3	1.6	1.3	2.6
	θ_{max} (°)	11.7	38.6	75.3	56.1	81.1

θ_{max} is measured anticlockwise from x-axis in degrees.

upper Formation 2 reflects the formation anisotropy. Owing to the low effective porosity values and the relatively high fracture density, particle travel times through the host rock are short. The mean particle travel time from the repository to the seabed is only 123 years when a constant hydraulic aperture of 10 μm is used. This is a remarkably short time period and represents an extreme case where the whole of the

geological setting is comprised of strong and coherent rock materials. This is unrealistic given the mechanical variability of most fractured rocks observed over typical transport scales. Nevertheless, it provides a useful comparison with the mechanical base case and highlights the importance of fracture mechanical strength on the flow and transport properties of the host and overlying formations.

The results for the particle travel times for various constant hydraulic apertures and fracture densities from the repository to the seabed are presented graphically in Fig. 13. For the low fracture density case, the hydraulic conductivity estimated for a block size of 25 m × 25 m has been used even though this size does not correspond to the REV, which is estimated to be greater than 100 m × 100 m. This block size does allow a calculation of the mechanical closure of the fracture apertures for the HM case and therefore a comparison of the results can be made between the two cases for low-density conditions. The results of the continuum model, based upon constant hydraulic apertures, display very short mean particle travel times from the repository to the seabed. For example, for the low and high fracture density networks, adopting a constant hydraulic aperture of 10 μm, particle travel times from the repository to the seabed are 580 years and 106 years, respectively. A doubling of the aperture increases the conductivity by a factor of eight and increases the porosity by a factor of two if the cubic law is adopted. This leads to an overall increase in velocity of a factor of four. Errors in velocity are therefore related to the square of the errors in the estimation of the hydraulic aperture. This sensitivity is clearly important in determining the accuracy of any travel time modelling and appropriate ranges for hydraulic aperture.

4.2. Mean HM base case

For the HM base case, only the mean mechanical properties have been used to calculate the hydraulic aperture distributions over the depth of the model for each of the density cases. The continuum model and the
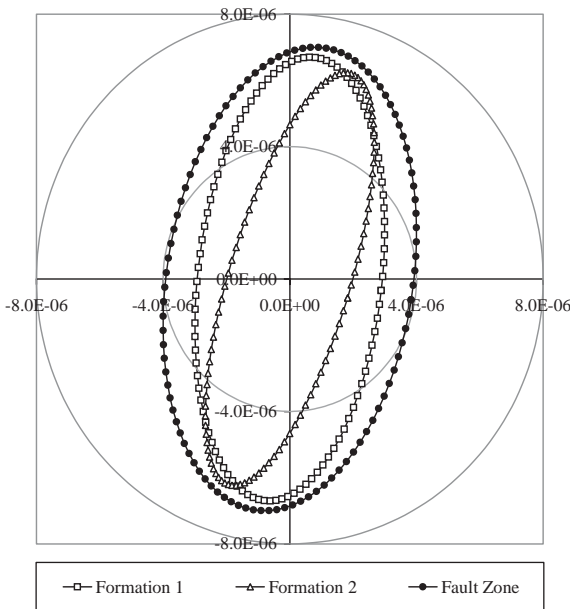

Fig. 11. Hydraulic conductivity ellipses for the three rock formations. Calculation based upon a block size of 10 m × 10 m, medium fracture density, and uniform hydraulic aperture of 50 μm.

Table 4
Summary of the average effective porosity for the mechanical parameter set 1

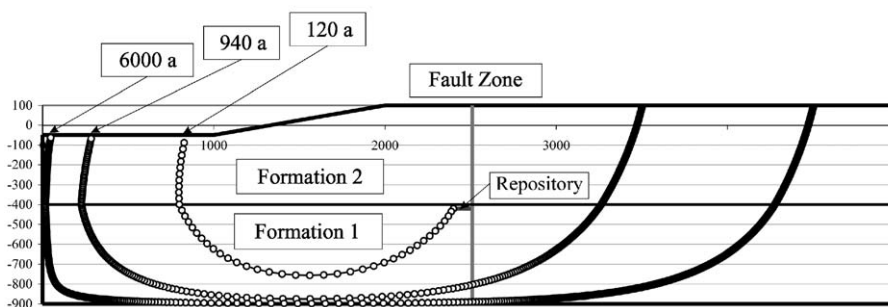| Depth:	25 m	75 m	175 m	375 m	750 m
Formation					
F1	1.7×10^{-4}	1.5×10^{-4}	1.2×10^{-4}	1.0×10^{-4}	9.1×10^{-5}
F2	5.9×10^{-6}	4.8×10^{-6}	2.6×10^{-6}	1.5×10^{-6}	—
FZ	1.3×10^{-4}	1.3×10^{-4}	1.2×10^{-4}	1.2×10^{-4}	9.2×10^{-5}

Fig. 12. Hypothetical host rock with streamlines and particle travel times for the hydraulic base case (medium fracture density with constant hydraulic aperture of 10 μm).
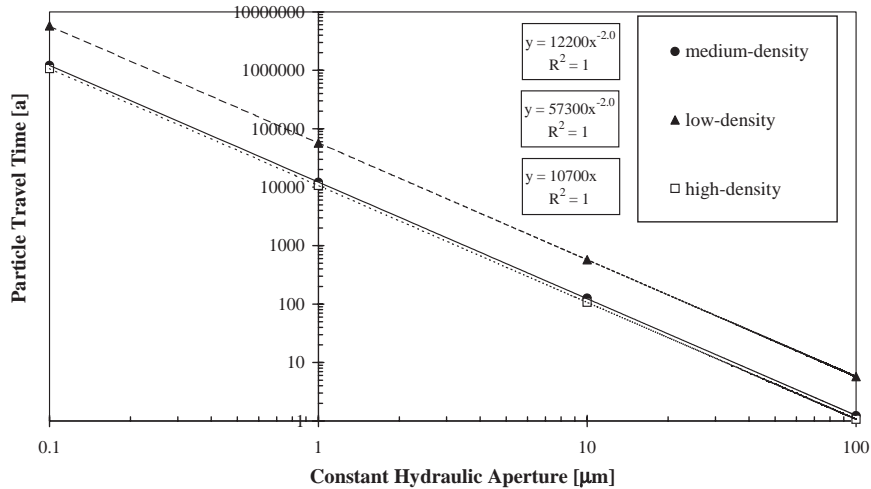
Fig. 13. Summary of the particle travel times from the repository to the seabed for a range of uniform hydraulic apertures and fracture densities.
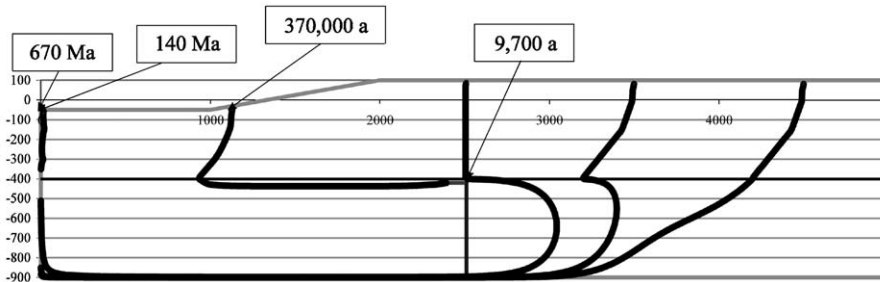

Fig. 14. Hypothetical host rock with streamlines and particle travel times for the HM base case.

applied methodology for the HM coupling in fractured rock does not allow the modelling of a fully HM coupled system, hence the HM modified hydraulic conductivity tensors were calculated at the mid point values of several depth ranges (Table 1). The results were assigned uniformly to the formation within each depth range (0–50 m, 50–100 m, 100–250 m, 250–500 m and 500–1000 m). The variation in the calculated aperture values decreases as depth increases, which allows for the larger depth bands at the base of the model.

The result for the mean HM base case is shown in Fig. 14. An additional particle trajectory starting at the top of the fault Zone is also presented. The streamlines reveal a quite different geometry to the *H* base case. The impact of the presence of the fault is clear and the impact of the anisotropy of Formation 2 is apparent. Locally the aperture anisotropy increases the particle travel time. The increase to 370 000 years for the particle travel time from the repository to the seabed from the *H* base case is predominantly caused by the very tight upper Formation 2 with an average hydraulic aperture for the entire formation of around 0.14 μm. The low conductivity upper formation significantly reduces the total flow through the whole system, which consequently lowers the fluid velocities through the host rock.

The mean particle travel time down the higher conductivity fault zone from the ground surface to the top of Formation 1 only takes around 9700 years, showing that the fault zone can act as a conductive pipe connecting the surface to the lower formation and influencing the flow geometry when the upper formation is tight. The very low flow contributions from the right-hand side of the model to the flow regime are illustrated by the closely spaced, near vertical trajectories adjacent to the left-hand boundary of the particles starting from the right-hand side. This further indicates the strong influence of the tight Formation 2 coupled to the conductive fault.

5. Discussion

The results of the HM modelling using the UDEC–BB calculated hydraulic aperture distributions under different stress conditions demonstrate the importance of the mechanical properties and their spatial variations in the rock mass on the hydraulic

behaviour of the rock mass. The large-scale studies show the strong dependency of the travel times within the different formations on the effective porosities and hydraulic conductivities. At this stage, only the mean mechanical property values have been used in the continuum model, thus the impact of the spatial distribution of the entire range of observed mechanical properties has still to be assessed. The lack of precise knowledge about the distribution of the mechanical properties in the host rock and the large variability observed in the field data indicate that a stochastic approach is essential. However, unless verifiable models of the spatial patterns of the mechanical properties can be developed and sufficient data collected to support the use of these models, it is likely that very large uncertainty in the modelling of travel times in fractured formations will remain in the future.

The outcome of this study demonstrates the impact of different fracture densities on the large-scale analysis. The comparison between the medium and high fracture density case with a constant aperture of 10 μm revealed a change in the particle travel time from the repository to the seabed of only 17 years (123–106 years), which appears to be modest compared with the impact on travel times of changing the mechanical properties, and therefore the apertures. Variations in the mechanical properties can change the aperture distribution of a formation by up to two orders of magnitude and thus can change the particle travel time by up to four orders of magnitude. This change in particle travel times is not possible by changing only the fracture density within the range of uncertainty identified by the data. Hence, the results suggest that, in the context of a performance assessment of deep waste disposal, the impact caused by the uncertainty in the spatial distribution of mechanical properties is probably of much greater significance than that caused by the spatial distribution of the fracture densities. Although potentially reasonable for the mean density cases, for the low-density case, where no REV could be obtained, this conclusion may be invalid due to the potential for the total loss of connectivity of the fracture network at the large scale.

6. Conclusions

The methodology for upscaling HM processes from the small scale (metre scale) to the large scale (kilometre scale) has been used to assess the importance of HM processes in performance assessment of deep waste disposal. The results reveal a wide range of potential hydraulic aperture distributions in the rock mass and a strong sensitivity of the hydraulic apertures to the mechanical properties of the rock mass and the fractures. The median hydraulic apertures ranged from 0.05 to 180.7 μm depending on the mechanical

properties and the applied stresses. The HM modelling of all three formations showed a non-linear decrease in the hydraulic aperture distribution with increasing depth. Further, it demonstrated that at low- stress values (corresponding to depths less than 250 m) the anisotropy of the hydraulic conductivity is dependent on the fracture orientation. The aperture anisotropy can influence the flow direction and the particle travel times but that this effect has less significance than the mechanical variations, which can most strongly influence the particle travel times.

The main conclusions drawn from the small- and large-scale analyses are that in the context of HM coupling, the different mechanical properties and their spatial variations are the most important factors in performance assessment of deep waste disposal followed by the uncertainty of the fracture density and the spatial distribution of the fracture density.

References

[1] Koltermann CE, Gorelick SM. Heterogeneity in sedimentary deposits: a review of structure-imitating, process-imitating, and descriptive approaches. Water Resour Res 1996;32(9):2617–58.

[2] Jackson CP, Hoch AR, Todman S. Self-consistency of a heterogeneous continuum porous medium representation of fractured media. Water Resour Res 2000;36(1):189–202.

[3] Martin CD, Davison CC, Kozak ET. Characterizing normal stiffness and hydraulic conductivity of a major shear zone in granite. In: Barton, Stephansson, editors. Rock joints. Rotterdam: Balkema; 2000. p. 549–56.

[4] Eidsvig UMK. Stress-dependent permeability in fractured rock. In: 3rd Euroconference on rock physics and rock mechanics, Bad Honnef, Germany; 2000.

[5] Nirex, An assessment of the post-closure performance of a deep waste repository at Sellafield. Nirex science report, S/97/012, Harwell, UK; 1997.

[6] Long JCS, Remer JS, Wilson CR, Witherspoon PA. Porous media equivalents for networks of discontinuous fractures. Water Resour Res 1982;18(3):645–58.

[7] Nirex. Evaluation of heterogeneity and scaling of fractures in the Borrowdale Volcanic Group in the Sellafield area. Nirex report SA/97/028, Harwell, UK; 1997.

[8] Endo HK, Long JCS, Wilson CR, Witherspoon PA. A model for investigating mechanical transport in fracture networks. Water Resour Res 1984;20(10):1390–400.

[9] Bandis SC, Lumsden AC, Barton NR. Fundamentals of rock joint deformation. Int J Rock Mech Min Sci Geomech Abstr 1983;20(5):249–68.

[10] Barton N, Bandis S, Bakhtar K. Strength, deformation and conductivity coupling of rock joints. Int J Rock Mech Min Sci Aeromech Abstr 1985;22(3):121–40.

[11] Nirex. Assessment of the in situ stress field at Sellafield. Nirex report S/97/003, Harwell, UK; 1997.

[12] NGI. Geotechnical (CSFT) laboratory testing of BVG joint samples from boreholes RCF1 and RCF3. NGI report No. 931005-102/2; 1993.

[13] Brace WF. Permeability of argillaceous and crystalline rocks. Int J Rock Mech Min Sci Geomech Abstr 1980;17:241–51.

[14] Armitage P, Holton D, Jefferies NL, Myatt BJ, Wilcock PM. Groundwater flow through fractured rock at Sellafield. European Science, Nuclear Science and Technology, EUR 16870 EN; 1996.